Two- and one-photon absorption spectra of aqueous thiocyanate anion highlight the role of symmetry in condensed phase

Ronit Sarangi, Kaushik Nanda, and Anna I. Krylov*
Department of Chemistry, University of Southern California, Los Angeles, CA 90089, U.S.A.[a)]

Calculation of the two-photon (2PA) absorption spectrum of aqueous thiocyanate using high-level quantum-chemistry methods is presented. The 2PA spectrum is compared to the 1PA spectrum computed using the same computational protocol. Although the two spectra probe the same set of electronic states, the intensity patterns are different, leading to an apparent red-shift of the 2PA spectrum relative to the 1PA spectrum. The presented analysis explains the intensity patterns and attributes the differences between 1PA and 2PA to the native symmetry of isolated SCN^-, which influences the spectra in the low-symmetry solution environment. The native symmetry also manifests itself in variations in the polarization ratio (e.g., parallel versus perpendicular cross sections) across the spectrum. The presented results highlight the potential of the 2PA spectroscopy and high-level quantum-chemistry methods in studies of condensed-phase phenomena.

I. INTRODUCTION

Spectroscopy in the condensed phase reveals both the electronic structure of solvated molecules and the details of the local solvent structure around the solute. Particularly sensitive to the solvent structure are the charge-transfer-to-solvent (CTTS) states[1–3]. These states, common for anionic solutes, are derived by promoting an electron from a molecular orbital to a proximal solvent cavity. The shapes of the molecular orbitals occupied by the excited electron resemble solvated electrons; however, in CTTS states, the excited electron interacts with the molecular core, making these states optically accessible. They appear as broad and featureless bands in the deep UV region (above 5 eV) of many solvated anions. Because of the diffuse nature of the excited electron, the energies and oscillator strengths of CTTS states depend strongly on the size and shape of the solvent cavity around the solute. Importantly, these states are highly sensitive to dynamic structural fluctuations of the solvent around the solute. This sensitivity leads to the strong solvent, temperature, and pressure dependence of the CTTS bands[3,4]. Furthermore, owing to this sensitivity, spectroscopies involving CTTS states can be used to probe the local structure of the solvent around anions and its dynamic fluctuations. However, to relate experimental spectra to microscopic structural information, theoretical modeling is required.

Recently, we presented a computational study of aqueous thiocyanate[5] using high-level electronic structure methods. We investigated the sensitivity of the computed UV–visible (UV–vis) spectra to the details of computational protocol, notably, equilibrium sampling. In particular, we found that molecular dynamics (MD) simulations using classical force fields produced more confined local structures around the thiocyanate anions as compared to more accurate simulations using *ab initio* MD combined with electrostatic embedding. Consequently, the spectra computed using these two sets of snapshots were markedly different, despite the inhomogeneous broadening of the transitions. Hence, the combination of theory and experiments can be used to validate and improve theoretical methods for condensed-phase modeling.

In this contribution, we compute and analyze the two-photon absorption (2PA) spectrum of $SCN^-_{(aq)}$ using the same computational protocol as in calculations of the one-photon absorption (1PA) spectrum. Non-linear spectroscopies, such as 2PA, second-harmonic generation, electronic sum-frequency generation (SFG), are gaining popularity, including applications to solvated anions[6–10]. Because 1PA and 2PA transitions are governed by different selection rules, 2PA spectra can provide complementary information, for example, by revealing states that are dark in 1PA[11,12]. In addition, 2PA can provide more detailed information about the underlying electronic structure, such as the symmetry of electronic states of the solute, by varying the polarizations of the two photons[12–14]. For example, Bradforth and co-workers have shown that different electronic states of water can be discerned from polarization dependence of the continuous 2PA spectra of bulk water[15].

Although in solutions the formal symmetry is C_1, the native symmetry of the solvated species strongly influences their optical properties. For example, $n \rightarrow \pi^*$ transitions are rather dim in 1PA, despite being formally allowed. However, such dim transitions can be probed using a different spectroscopy. As a recent illustration of how such selection rules can be overcome by multiphoton techniques, consider the electronic spectrum of aqueous OH radical[16]. Its UV–vis spectrum shows only a small shoulder corresponding to the $\sigma(p_z) \rightarrow \pi(p_x/p_y)$ valence transition, but the same transitions become sharp in the RIXS (resonant inelastic X-ray scattering) spectrum[16].

As a linear molecule, SCN^- is an interesting model system for analyzing the effect of native symmetry on the 1PA and 2PA spectra in solutions. Here, we analyze the computed electronic states and their properties in terms of their relationship to hypothetical states of an ideal symmetric model. By comparing 1PA and 2PA spectra, we highlight the changes in the intensity patterns. Together with polarization data, such differences between 1PA and 2PA spectra can be used for spectroscopic assignments. We hope that our simulations will motivate experimental efforts to measure the continuous 2PA spectrum of this interesting system.

[a)]Electronic mail: krylov@usc.edu

The structure of the paper is as follows. We begin with a description of theoretical methods and computational protocols. We then discuss molecular orbital framework and symmetry analysis of the low-energy electronic states of aqueous thiocyanate. We then apply this analysis to explain trends in 1PA and 2PA spectra.

II. THEORETICAL METHODS AND COMPUTATIONAL DETAILS.

Ab initio modeling of condensed-phase spectroscopy requires the following: (i) quantum chemistry method capable of describing electronic states involved; (ii) an adequate description of the solute–solvent interactions; (iii) the ability to compute spectroscopic signal (e.g., absorption cross sections); (iv) reliable description of equilibrium dynamics; and (v) tools for spectroscopic assignments. Our previous study of aqueous thiocyanate[5] illustrates the challenges involved in developing computationally feasible protocols that adequately address these points. Below, we briefly summarize essential details of the theoretical framework and its extension to 2PA.

We use the equation-of-motion coupled-cluster method for electronically excited states with single and double substitutions (EOM-EE-CCSD), which is capable of treating states of different character (e.g., local and CTTS excitations) in a balanced way[17]. Describing solvent effects in calculations of electronic spectra of solvated anions is particularly difficult because, in addition to strong electrostatic interactions, one should also properly treat quantum confinement effects (Pauli repulsion between solvent molecules and excited electrons) that prevent the artificial spilling of the electron density of the solute into the solvent. Towards this end, we employ a relatively large QM system comprising the thiocyanate molecule and more than two solvation shells.

Whereas calculations of UV–vis (1PA) intensities is straightforward, the calculation of the 2PA cross sections requires implementation of response equations. Here, we use theoretical framework described in Refs. 18–20. We carried out equilibrium averaging using the same snapshots from the AIMD trajectories as were used in the calculations of 1PA spectra[5]. To assign the spectral features, we used wavefunction analysis and exciton descriptors[21–25], in particular, exciton sizes, which allow one to distinguish between local and CTTS excitations. For 2PA, we used the NTOs of the perturbed density[20], which are related to the 2PA transition moments.

We note that robust modeling of multiphoton properties such as 2PA cross sections is very sensitive to approximations in electron-correlation treatment[19,26]. The underlying model Hamiltonians must reliably describe not only the initial and final states in a transition but the full spectrum of electronic states, owing to the sum-over-states expressions of the corresponding cross-sections (see, for example, expressions for 2PA transition moments below). This is different from modeling one-photon spectroscopies (e.g., UV–vis) in which one only needs to compute transition dipole moments between the ground state and a few low-lying excited states. Therefore, electronic structure methods and computational protocols that provide a robust theoretical characterization of UV–vis spectra may be inadequate for 2PA spectra[19,26].

EOM-EE-CCSD has been used to model 2PA spectra of several isolated chromophores[18,27–30], showing a reasonable agreement with available experimental spectra despite neglecting the solvent effects, especially in non-polar solvents[28,29]. Coupled-cluster simulations using explicit solvent models have also been reported[19,31,32]. Here, we apply the EOM-EE-CCSD method combined with explicit solvent description to a system that is more demanding in terms of the description of the solute–solvent interactions. This is the first application of EOM-EE-CCSD for calculations of nonlinear optical spectra involving CTTS states. Once the experimental 2PA spectrum of $SCN^-_{(aq)}$ will become available, our simulations will serve as an important benchmark for assessing the performance of EOM-EE-CCSD combined with the explicit description of the solvent. These results can also be used for developing more approximate treatments for electron correlation and embedding.

A. 2PA cross sections within EOM-EE-CCSD framework

Below, we outline the theoretical framework for computing 2PA cross sections[18]. Within the non-Hermitian EOM-CC theory, the right and left transition moments are not equivalent. Using the expectation-value EOM-EE-CCSD formalism, the right and left 2PA transition moments ($M_{yz}^{f\leftarrow g}$ and $M_{yz}^{g\leftarrow f}$, respectively) are given by the sum-over-all-states expressions[18–20],

$$M_{yz}^{f\leftarrow g} = -\sum_n \frac{\langle\Phi_0|\hat{L}^f\hat{\mu}_z\hat{R}^n|\Phi_0\rangle\langle\Phi_0|\hat{L}^n\hat{\mu}_y\hat{R}^g|\Phi_0\rangle}{E^n-E^g-\omega_1} - \sum_n \frac{\langle\Phi_0|\hat{L}^f\hat{\mu}_y\hat{R}^n|\Phi_0\rangle\langle\Phi_0|\hat{L}^n\hat{\mu}_z\hat{R}^g|\Phi_0\rangle}{E^n-E^g-\omega_2} \tag{1}$$

and

$$M_{yz}^{g\leftarrow f} = -\sum_n \frac{\langle\Phi_0|\hat{L}^g\hat{\mu}_y\hat{R}^n|\Phi_0\rangle\langle\Psi_0|\hat{L}^n\hat{\mu}_z\hat{R}^f|\Phi_0\rangle}{E^n-E^g-\omega_1} - \sum_n \frac{\langle\Phi_0|\hat{L}^g\hat{\mu}_z\hat{R}^n|\Phi_0\rangle\langle\Phi_0|\hat{L}^n\hat{\mu}_y\hat{R}^f|\Phi_0\rangle}{E^n-E^g-\omega_2}, \tag{2}$$

respectively. Here, g, n, and f are state indices for the initial, intermediate, and final states. The energies E^k and right and left EOM-CC wave functions ($\hat{R}^k|\Phi_0\rangle$ and $\langle\Phi_0|\hat{L}^k$, respectively) of state k within the EOM-EE-CCSD framework are computed by solving the following right and left EOM-CC eigenvalue equations in the determinant space of the reference (Φ_0) and singly and doubly excited determinants:

$$\bar{H}\hat{R}^k|\Phi_0\rangle = E^k\hat{R}^k|\Phi_0\rangle \tag{3}$$

and

$$\langle\Phi_0|\hat{L}^k\bar{H} = \langle\Phi_0|\hat{L}^kE^k, \tag{4}$$

where $\bar{H} = e^{-\hat{T}} H e^{\hat{T}}$ is the EOM-CCSD similarity-transformed Hamiltonian expressed in terms of the CCSD operator, $\hat{T}$. The energies of the two photons (ωs) satisfy the 2PA resonance condition: $\Omega^{fg} = E^f - E^g = \omega_1 + \omega_2$. $\hat{\bar{\mu}}_x = e^{-\hat{T}} \bar{\mu}_x e^{\hat{T}}$ is the x Cartesian component of the similarity transformed dipole-moment operator. The 2PA transition moments are computed by recasting the sum-over-states expressions into expressions that use response states, which are computed with roughly the same cost as excited states themselves[18].

The rotationally averaged microscopic 2PA cross sections are computed using the transition strength matrix, $S_{ab,cd}$, as follows:

$$\langle \delta^{2PA} \rangle^{gf} = \frac{1}{30}\left(F\delta_F + G\delta_G + H\delta_H\right) = \frac{1}{30}\left(F\sum_{a,b} S^{gf}_{aa,bb} + G\sum_{a,b} S^{gf}_{ab,ab} + H\sum_{a,b} S^{gf}_{ab.ba}\right), \quad (5)$$

where $S_{ab,cd}$ is given in terms of the products of left and right 2PA transition-moment components,

$$S^{gf}_{ab,cd} = \frac{1}{2}\left((M^{g\leftarrow f}_{ab})^* M^{f\leftarrow g}_{cd} + (M^{g\leftarrow f}_{cd})^* M^{f\leftarrow g}_{ab}\right). \quad (6)$$

The constants F, G, and H depend on the polarization of the incident light[13]. $F = G = H = 2$ for parallel linearly polarized light, $F = -1$, $G = 4$, $H = -1$ for perpendicular linearly polarized light, and $F = -2$, $G = H = 3$ for circularly polarized light.

The macroscopic 2PA cross section, $\langle \sigma^{2PA} \rangle$ (in Göppert-Mayer units, 1 GM = 10^{-50} cm^{4}s/photon) are expressed in terms of $\langle \delta^{2PA} \rangle$ as

$$\langle \sigma^{2PA} \rangle^{gf}(\omega) = \frac{2\pi^3 \alpha a_0^5 \left(\Omega^{fg}\right)^2}{c} \langle \delta^{2PA} \rangle^{g\leftarrow f} \mathscr{L}\left(\Omega^{fg}, \omega, \Gamma\right), \quad (7)$$

where α is the fine structure constant, a_0 is the Bohr radius, c is the speed of light, and $\mathscr{L}(E^f - E^g, \omega, \Gamma)$ is the line-shape function (Γ is an empirical factor describing line broadening).

B. Polarization ratios

In their pioneering work, McClain and co-workers[13,14] explained by varying relative polarization of the two photons, one can discern the three contributions to the overall cross-section—δ_F, δ_G, and δ_H— and by doing so gain a more detailed picture of the underlying electronic structure. The most common approach is to compare the spectra obtained with parallel (σ_{par}) and perpendicular (σ_{perp}) polarizations of the two photons. Below we briefly summarize the key expressions[13].

For linearly polarized light:

$$\langle \delta \rangle = A + B\cos^2(\theta), \quad (8)$$

where θ is the angle between the two photons. Hence, the polarization ratio r of parallel and perpendicular cross sections is

$$r = \frac{\delta_{par}}{\delta_{per}} = 1 + \frac{B}{A} \quad (9)$$

For the degenerate 2PA, $\delta_G = \delta_H$ (this also holds for non-degenerate case for fully symmetric transitions)[13]. In these cases:

$$A = -\delta_F + 3\delta_G \quad (10)$$

$$B = 3\delta_F + \delta_G \quad (11)$$

As per Eq. (5), the expressions for δ_F and δ_G are:

$$\delta_F = \sum_{a,b} S_{aa,bb} = S_{xx,xx} + S_{xx,yy} + S_{xx,zz} + S_{yy,xx} + S_{yy,yy} + S_{yy,zz} + S_{zz,xx} + S_{zz,yy} + S_{zz,zz} \quad (12)$$

and

$$\delta_G = \sum_{a,b} S_{ab,ab} = S_{xx,xx} + S_{xy,xy} + S_{xz,xz} + S_{yx,yx} + S_{yy,yy} + S_{yz,yz} + S_{zx,zx} + S_{zy,zy} + S_{zz,zz}. \quad (13)$$

To apply these equations to a specific case, one needs to write down the structure of S, based on the properties of the 2PA moments (they are given in Ref. 14 for all symmetry groups). Below we do this for SCN^- ($C_{\infty v}$).

C. Computational Details

We computed the 2PA spectra using a hybrid QM/MM approach with an electrostatic embedding scheme in which the QM part was treated with EOM-EE-CCSD and the MM waters were described as Gaussian-broadened TIP3P point charges. As in the calculations of 1PA spectra[5], we constructed the spectra using eight excited states per snapshot (the benchmarks in Ref. 5 have shown that the computed 1PA spectrum does not change when up to 10 states per snapshot were computed). A total of 40 snapshots were chosen from the AIMD calculations performed in Ref. 5. The QM region consisted of SCN^- and 20 nearest waters with the 6-31+G* basis on the anion and 11 nearest waters and 6-31G on the rest. We carried out a non-degenerate 2PA calculation with ω_1 fixed at 4.66 eV. The line-shape function, $\mathscr{L}$, was a normalized Gaussian with FWHM of 0.1 eV. All calculations were performed using the Q-Chem software[33,34]. We provide a sample input for EOM-EE-CCSD 2PA jobs in the SI.

III. RESULTS AND DISCUSSION

We begin with discussing MO framework and symmetry of the electronic states of SCN^-. Although in the condensed phase the symmetry is C_1, MOs largely retain their shapes and nodal structures as can be easily seen from the actual computed orbitals, e.g., Fig. 3 in Ref. 5 and Fig. S1 in the SI.

Thus, the electronic states of $SCN^-_{(aq)}$ can be understood in terms of perturbed states of an isolated linear molecule.

Table I shows the character table for $C_{\infty v}$ group. It has an infinite number of irreducible representations (irreps), but for the low-lying electronic states of SCN^- only A_1, A_2, E_1, and E_2 are relevant. Fig. 1 shows the MOs involved in the low-lying electronic transitions of SCN^-: doubly degenerate HOMO of π character (E_1/Π), doubly degenerate LUMO of π^* character (E_1/Π), and four diffuse atomic-like orbitals—s (A_1/Σ^+), p_z (A_1/Σ^+), and p_x/p_y (E_1/Π).

TABLE I. Character table for $C_{\infty v}$ group with standard and spectroscopic irrep labels.

Irrep	E	$2C_\infty$	$\infty\sigma_v$	Lin. fns.
A_1/Σ^+	1	1	1	z
A_2/Σ^-	1	1	-1	
E_1/Π	1	$2\cos(\phi)$	0	x,y
E_2/Δ	1	$2\cos(2\phi)$	0	
E_3/Φ	1	$2\cos(3\phi)$	0	
E_n	1	$2\cos(n\phi)$	0	

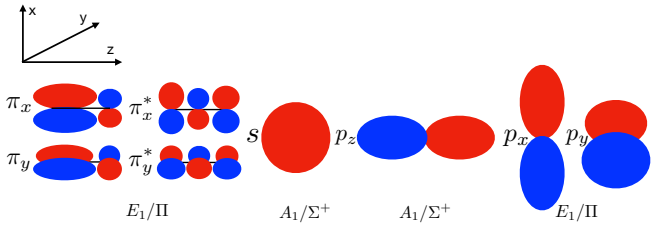

FIG. 1. Relevant molecular orbitals of SCN^- and their symmetry labels (in $C_{\infty v}$ group).

The ground electronic state of SCN^- is $X^1\Sigma^+$. Isolated thiocyanate anion does not support bound electronic states, but in aqueous solutions the detachment energy increases considerably and several excited states become electronically bound. The low-lying states of aqueous SCN^- are derived from the transitions between the doubly degenerate π HOMO and doubly degenerate π^* LUMO, giving rise to the intramolecular excitations, and transitions from the HOMO to the diffuse atomic-like orbitals (s, p_x, p_y, and p_z), giving rise to the CTTS transitions. The CTTS transitions can mix with the locally excited transitions. In the absence of symmetry, all transitions can mix, however, as we observe from the calculations, many states have character that can be assigned to a particular type of transition. This can be seen from the shapes of NTOs, and even more so, from the electronic properties (e.g., oscillator strengths). As we show below, this native symmetry also explains trends in the 2PA spectrum.

Table II shows the symmetries of electronic states derived from transitions between orbitals from Fig. 1 (see Table S1 in the SI for the irrep multiplication table). There are total of twelve configurations that can be generated of which six are dipole allowed—one local transition and five CTTS transitions. We note that the NTO analysis only shows the nature of the orbitals involved, but does not distinguish between different symmetries—for example, all local excitations have two

TABLE II. Symmetry analysis of electronic transitions. The polarization of transitions is shown in parentheses.

Transition	Symmetry/States	# states	1PA allowed
$\pi \to \pi^*$	$\Pi\times\Pi \to \Sigma^+ + \Sigma^- + \Delta$	4	Σ^+ (z)
$\pi \to s$	$\Pi\times\Sigma^+ \to \Pi$	2	Π (x,y)
$\pi \to p_z$	$\Pi\times\Sigma^+ \to \Pi$	2	Π (x,y)
$\pi \to p_x/p_y$	$\Pi\times\Pi \to \Sigma^+ + \Sigma^- + \Delta$	4	Σ^+ (z)

pairs of similar looking NTOs. Different states can be distinguished by either wave-function amplitudes or by the transition properties such as transition dipole moments or matrix elements of the angular momentum operator.

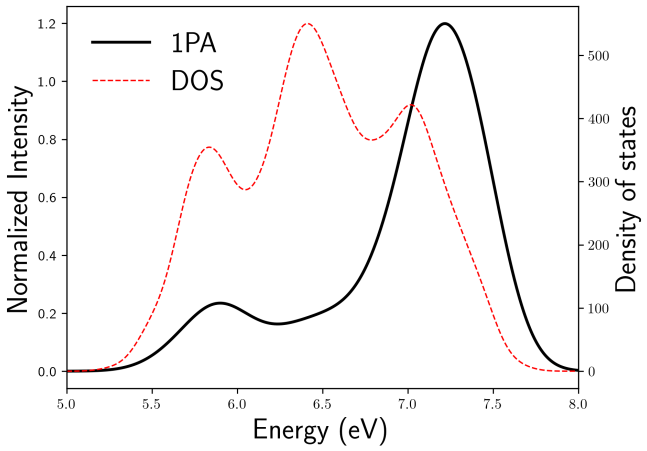

FIG. 2. Density of states and 1PA spectrum computed using 8 states from AIMD snapshots.

The calculations of the spectra are based on eight lowest exited states, which was deemed sufficient for capturing the low-energy part of the 1PA spectrum[5]. Fig. 2 shows the computed density of states and the 1PA spectrum. As one can see, eight states span energy range of about 2 eV and are clustered in three groups—around 5.7 eV, 6.5 eV, and 7.2 eV, with the second group being the largest. However, the intensities of the 1PA spectrum are completely different—the most intense peak corresponds to the third group and has a maximum at about 7.5 eV, the first peak has much lower intensity, and the second cluster of states gives rise to a shoulder in between the first and the third peaks. Such significant difference between the density of states and 1PA intensities is the result of the symmetry-imposed selection rules of the underlying transitions.

Based on the gas-phase calculations, the only bright locally excited state, Σ^+, lies several eV above the lowest excited state. In the condensed-phase calculations, we found no signatures of this bright $\pi\pi^*$ transition in the eight lowest states—the three states with predominant locally excited $\pi\pi^*$ character have very low oscillator strengths.

The NTO analysis shows that the intense bands in the 1PA spectrum correspond to the states with CTTS character. From Table II, we see that not all CTTS transitions are bright–among the eight transitions only five are dipole allowed; those

are doubly degenerate $\pi \rightarrow s$ and $\pi \rightarrow p_z$ (with transition dipole moment perpendicular to the molecular axis) and one $\pi \rightarrow p_x/p_y$ (with the transition dipole moment parallel to the molecular axis).

Fig. 3 shows exciton sizes for the eight states averaged over the equilibrium trajectory[5]. As one can see, states 3–5 have smaller sizes, so that they can be classified as predominantly local excitations, whereas states 1–2 and 6–8 have larger sizes. Thus, the lowest eight transitions in our condensed-phase calculations can be described as three dim local excitations, giving rise to the shoulder in the middle, and five brighter states of CTTS character, giving rise to the two brighter peaks, with the brightest peak having the largest CTTS character. Inspection of NTOs (see Fig. S1 in the SI and Ref. 5) shows that the third band is dominated by $\pi \rightarrow p_x/p_y$ transitions, whereas the lower band is due to $\pi \rightarrow s$ transitions. Additionally, the NTOs reveal some mixing between local and CTTS excitations in the two lower bands. We note that this mixing depends strongly on the local structure of the solvent and is not captured by the MD simulations using classical force fields.

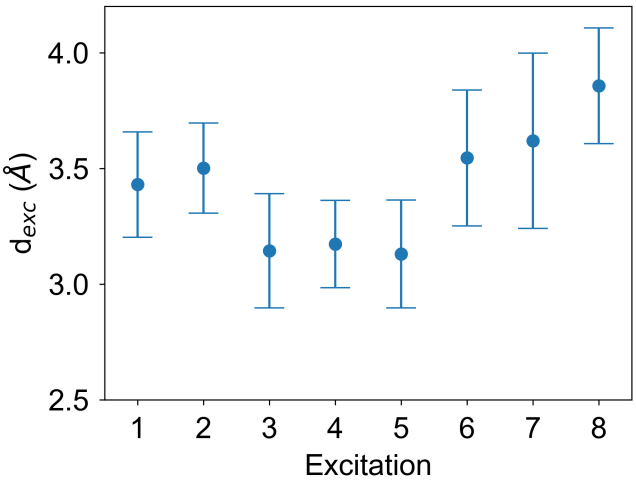

FIG. 3. Average exciton sizes and standard deviations for the eight lowest states of $SCN^-_{(aq)}$ computed using AIMD snapshots.

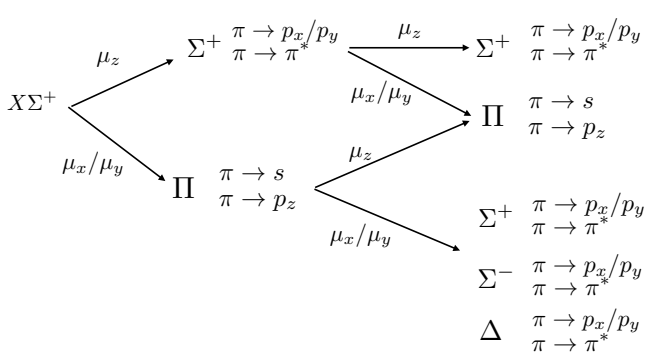

FIG. 4. Selection rules for 2PA transitions in SCN^-.

Fig. 4 summarizes symmetry-imposed selection rules for the manifold of low-lying electronic states in SCN^-. Dipole-allowed transitions are those for which product of the irreps of the initial and final state and dipole moment contains fully symmetric irrep (see Table S1 in the SI for help). As one can see, the dipole-forbidden Δ and Σ^- states become two-photon allowed, which should lead to the intensity increase in the low-energy part of the spectrum relative to 1PA.

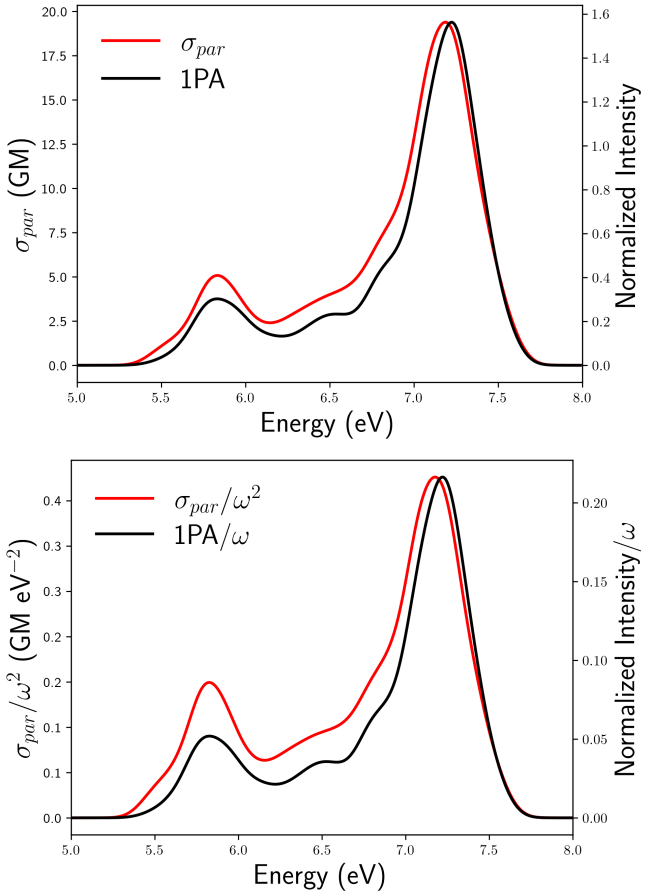

FIG. 5. Top panel: 1PA and 2PA (σ_{par}) spectra of aqueous SCN^-. Low panel: Energy-rescaled intensities: 1PA spectrum divided by the excitation energy (ω) and the 2PA spectrum divided by ω^2.

Fig. 5 compares the 1PA and 2PA (σ_{par}) spectra of aqueous SCN^-. As one can see, the relative intensities of the three bands change in 2PA, with the lower-energy peaks becoming more prominent, as anticipated from the symmetry considerations. The change becomes even more visible if one takes into account the frequency factor (Fig. 5, bottom panel), which favors higher-energy transitions—i.e., the oscillator strength is proportional to ω and the macroscopic 2PA cross section is proportional to ω^2.

The changes in the intensities result in an apparent red shift of ~0.05 eV of the three bands in 2PA relative to 2PA. This red shift is a purely electronic phenomenon, as the position of the excited states are the same in the two calculations, akin to the non-Condon effects observed in fluorescent proteins[35].

To further analyze the 2PA spectrum, we carried out NTO analysis of the 2PA response one-particle transition density matrices (1PTDM)[20]. In contrast to regular NTOs, which are

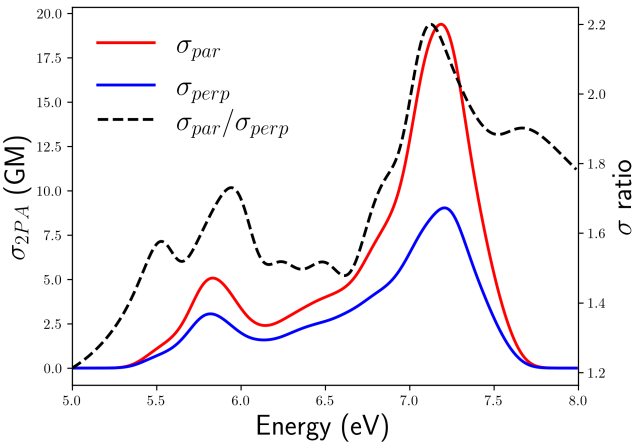

FIG. 6. Polarization of the 2PA spectra: σ_{par} and σ_{perp} and their ratio.

related to the 1PA intensities, these response (or 2PA) NTOs are related to the magnitude of the 2PA cross sections, so they can reveal the nature of the "virtual" state[36], providing details of the important orbitals involved in the 2PA transition. Figs. S1–S5 in the SI show 1PA and 2PA NTOs for a representative snapshot. For this snapshot, the first two transitions have clear *s*-type CTTS character and the next three transitions are intramolecular, and the last three are the *p*-type CTTS transitions. This characterization is based on the analysis of the dominant NTO pair of the 1PA 1PTDMs in Fig. S1 in the SI.

For the 2PA transitions, the response 1PTDMs have three Cartesian components and depend on frequencies of the two photons, which makes the analysis more involved. Figs. S2-S4 in the SI shows the 2PA NTOs. Qualitatively, we observe that these NTOs show contributions of multiple "virtual" states into the 2PA cross sections, which are not seen in 1PA NTOs. For example, for the first two transitions (Fig. S2 in the SI), the response 1PTDMs reveal dominant $\pi \rightarrow$ CTTS p_y NTO pair. We also observe a $\pi \rightarrow$ CTTS p_z character from the less important z-component response 1PTDMs.

Symmetry also affects the difference between the 2PA spectra obtained with parallel (σ_{par}) and perpendicular (σ_{perp}) polarized beams[12–14]. In general, the ratio is larger for fully symmetric transitions[12–14]. Following McClain[11,12], we can estimate the ratio r for our system using idealized symmetry ($C_{\infty v}$). Table III summarizes the symmetry-imposed structure of the 2PA moments for the $C_{\infty v}$ group.

For fully symmetric transition, $\Sigma^+ \rightarrow \Sigma^+$, we obtain

$$\delta_F = 2S_{xx,xx} + S_{zz,zz} + 4S_{xx,zz} + 2S_{xx,yy} \tag{14}$$

and

$$\delta_G = 2S_{xx,xx} + S_{zz,zz} + 4S_{xz,xz} + 2S_{xy,xy}, \tag{15}$$

TABLE III. Structure 2PA moments for transitions in $C_{\infty v}$ group[14].

Transition	Non-zero elements	Notes[a]
$\Sigma^+ \rightarrow \Sigma^+$	M_{zz}, M_{xx}, M_{yy}	$M_{xx} = M_{yy}$
$\Sigma^+ \rightarrow \Sigma^-$	M_{xy}, M_{yx}	$M_{xy} = -M_{yx}$
$\Sigma^+ \rightarrow \Pi$	$M_{xz}, M_{yz}, M_{zx}, M_{zy}$	$M_{yz} = -iM_{xz}, M_{zy} = -iM_{zx}$
$\Sigma^+ \rightarrow \Delta$	$M_{xx}, M_{xy}, M_{yx}, M_{yy}$	$M_{xy} = -iM_{xx}, M_{yy} = -M_{xx}$, $M_{yx} = -iM_{xx}$

[a] This is valid within Hermitian framework. For Π and Δ, there are two components and the moment for the second component is complex-conjugate of the other.

which yields

$$\begin{aligned} A = &-(2S_{xx,xx} + S_{zz,zz} + 4S_{xx,zz} + 2S_{xx,yy}) + \\ &3(2S_{xx,xx} + S_{zz,zz} + 4S_{xz,xz} + 2S_{xy,xy}) = \\ &4S_{xx,xx} + 2S_{zz,zz} + 12S_{xz,xz} + 6S_{xy,xy} - 4S_{xx,zz} - 2S_{xx,yy} = \\ &(4S_{xx,xx} + 2S_{zz,zz} + 6S_{xx,zz} + 3S_{xx,yy} + 2S_{xz,xz} + S_{xy,xy}) + \\ &(10S_{xz,xz} + 5S_{xy,xy} - 10S_{xx,zz} - 5S_{xx,yy}) \end{aligned} \tag{16}$$

and

$$\begin{aligned} B = &3(2S_{xx,xx} + S_{zz,zz} + 4S_{xx,zz} + 2S_{xx,yy}) + \\ &2S_{xx,xx} + S_{zz,zz} + 4S_{xz,xz} + 2S_{xy,xy} = \\ &8S_{xx,xx} + 4S_{zz,zz} + 12S_{xx,zz} + 6S_{xx,yy} + 4S_{xz,xz} + 2S_{xy,xy} = \\ &2(4S_{xx,xx} + 2S_{zz,zz} + 6S_{xx,zz} + 3S_{xx,yy} + 2S_{xz,xz} + S_{xy,xy}). \end{aligned} \tag{17}$$

Neglecting $(10S_{xz,xz} + 5S_{xy,xy} - 10S_{xx,zz} - 5S_{xx,yy})$ terms, we obtain $B/A \approx 2$, giving rise to $r \approx 3$.

For Σ^-, Π, and Δ transitions, δ_F=0, which gives $B/A = 1/3$ and $r = 4/3$.

The computed polarization ratio follows these idealized symmetry-based estimates. The ratio is the largest, reaching the value of 2.2, in region III, dominated by totally symmetric (Σ^+), $\pi \rightarrow p_x/p_y$ transitions. For other transitions, r varies between 1.4-1.7. The deviations from the limiting values of 3 (for Σ^+) and 1.3 (for Σ^+, Π, and Δ) can be explained by mixing configurations of different types and by the fact that the two photons are not degenerate.

We conclude by noting that the computed spectra (Fig. 6) show that the ratio shows more detailed structure than each spectrum alone, with about seven distinct peaks.

IV. CONCLUSIONS

Non-linear spectroscopies such as 2PA and SFG can provide complementary information of the electronic structure relative to linear (i.e., UV–vis) spectroscopy owing to their different selection rules. By using aqueous thiocyanate, we demonstrated that the symmetry-imposed selection rules of the ideal (isolated) system persist in the condensed-phase and strongly influence 1PA and 2PA spectral features.

We have presented state-of-the-art simulations of the 2PA spectra of $SCN^-_{(aq)}$ and compared it with the 1PA spectrum

computed using the same protocol. The simulations reveal changes in the intensity patterns, which can be explained by the native symmetry of the solute. The native symmetry leads to the variations of polarization ratio across the 2PA spectrum, which can facilitate spectroscopic assignments. These changes in the intensities result in an apparent red shift of the 2PA spectrum of 0.05 eV relative to 1PA. We emphasize that the electronic states probed in both experiments are the same and the shift is of purely electronic nature, akin to non-Condon effects observed in fluorescent proteins[35].

Our study contributes to a growing body of non-linear spectroscopic studies in condensed phase. We hope that our results will inspire future spectroscopic studies on this system and provide useful benchmark for theoretical developments.

ACKNOWLEDGMENTS

This work was supported by the U.S. National Science Foundation (No. CHE-2154482 to A.I.K.)

CONFLICTS OF INTEREST

The authors declare the following competing financial interest(s): A.I.K. is the president and a part-owner of Q-Chem, Inc.

[1]Smith, M.; Symons, M. C. R. Solvation spectra. Part 1. The effect of environmental changes upon the ultra-violet absorption of solvated iodide ions *Trans. Faraday Soc.* **1958**, *54*, 338–345.
[2]Stein, G.; Treinin, A. Electron-transfer spectra of anions in solution. Part 1. Absorption spectra and ionic radii *Trans. Faraday Soc.* **1959**, *55*, 1086–1090.
[3]Blandamer, M.J.; Fox, M.F. Theory and applications of charge-transfer-to-solvent spectra *Chem. Rev.* **1970**, *70*, 59–93.
[4]Griffiths, T. R.; Symons, M. C. R. Solvation spectra. Part 3. Further studies of the effect of environmental changes on the ultra-violet spectrum of iodide ions *Trans. Faraday Soc.* **1960**, *56*, 1125–1136.
[5]Sarangi, R.; Nanda, K. D.; Krylov, A. I. Charge-transfer-to-solvent states provide a sensitive spectroscopic tool to probe local structure of water around solvated anions *Mol. Phys.* **2023**, *121*, e2148582.
[6]Petersen, P. B.; Saykally, R. J.; Mucha, M.; Jungwirth, P. Enhanced concentration of polarizable anions at the liquid water surface: SHG spectroscopy and MD simulations of sodium thiocyanide *J. Phys. Chem. B* **2005**, *109*, 10915–10921.
[7]Onorato, R. M.; Otten, D.; Saykally, R. J. Adsorption of thiocyanate ions to the dodecanol/water interface characterized by UV second harmonic generation *Proc. Nat. Acad. Sci.* **2009**, *106*, 15176–15180.
[8]Rizzuto, A. M.; Irgen-Gioro, S.; Eftekhari-Bafrooei, A.; Saykally, R. J. Broadband deep UV spectra of interfacial aqueous iodide *J. Phys. Chem. Lett.* **2016**, *7*, 3882–3885.
[9]Mizuno, H.; Rizzuto, A. M.; Saykally, R. J. Charge-transfer-to-solvent spectrum of thiocyanate at the air/water interface measured by broadband deep ultraviolet electronic sum frequency generation spectroscopy *J. Phys. Chem. Lett.* **2018**, *9*, 4753–4757.
[10]Bhattacharyya, D.; Mizuno, H.; Rizzuto, A.M.; Zhang, Y.; Saykally, R. J.; Bradforth, S. E. New insights into the charge-transfer-to-solvent spectrum of aqueous iodide: Surface versus bulk *J. Phys. Chem. Lett.* **2020**, *11*, 1656–1661.
[11]McClain, W. M. Two-photon molecular spectroscopy *Acc. Chem. Res.* **1974**, *7*, 129–135.
[12]Wirth, M.J.; Koskelo, A.; Sanders, M.J. Molecular symmetry and 2-photon spectroscopy *Appl. Spectr.* **1981**, *35*, 14–21.
[13]Monson, P. R.; McClain, W. M. Polarization dependence of the two-photon absorption of tumbling molecules with application to liquid 1-chloronaphthalene and benzene *J. Chem. Phys.* **1970**, *53*, 29.
[14]McClain, W. M. Excited state symmetry assignment through polarized two-photon absorption studies of fluids *J. Chem. Phys.* **1971**, *55*, 2789–2796.
[15]Elles, C.G.; Rivera, C.A.; Zhang, Y.; Pieniazek, P.A.; Bradforth, S.E. Electronic structure of liquid water from polarization-dependent two-photon absorption spectroscopy *J. Chem. Phys.* **2009**, *130*, 084501.
[16]Kjellsson, L.; Nanda, K. D.; Rubensson, J.-E.; Doumy, G.; Southworth, S. H.; Ho, P. J.; March, A. M.; Al Haddad, A.; Kumagai, Y.; Tu, M.-F.; Debnath, T.; Bin Mohd Yusof, M. S.; Arnold, C.; Schlotter, W. F.; Moeller, S.; Coslovich, G.; Koralek, J. D.; Minitti, M. P.; Vidal, M. L.; Simon, M.; Santra, R.; Loh, Z.-H.; Coriani, S.; Krylov, A. I.; Young, L. Resonant inelastic x-ray scattering reveals hidden local transitions of the aqueous OH radical *Phys. Rev. Lett.* **2020**, *124*, 236001.
[17]Krylov, A. I. Equation-of-motion coupled-cluster methods for open-shell and electronically excited species: The hitchhiker's guide to Fock space *Annu. Rev. Phys. Chem.* **2008**, *59*, 433–462.
[18]Nanda, K. D.; Krylov, A. I. Two-photon absorption cross sections within equation-of-motion coupled-cluster formalism using resolution-of-the-identity and Cholesky decomposition representations: Theory, implementation, and benchmarks *J. Chem. Phys.* **2015**, *142*, 064118.
[19]Nanda, K. D.; Krylov, A. I. The effect of polarizable environment on two-photon absorption cross sections characterized by the equation-of-motion coupled-cluster singles and doubles method combined with the effective fragment potential approach *J. Chem. Phys.* **2018**, *149*, 164109.
[20]Nanda, K. D.; Krylov, A. I. Visualizing the contributions of virtual states to two-photon absorption cross-sections by natural transition orbitals of response transition density matrices *J. Phys. Chem. Lett.* **2017**, *8*, 3256–3265.
[21]Luzanov, A. V.; Sukhorukov, A. A.; Umanskii, V. E. Application of transition density matrix for analysis of excited states *Theor. Exp. Chem.* **1976**, *10*, 354–361; Russian original: Teor. Eksp. Khim., 10, 456 (1974).
[22]Bäppler, S. A.; Plasser, F.; Wormit, M.; Dreuw, A. Exciton analysis of many-body wave functions: Bridging the gap between the quasiparticle and molecular orbital pictures *Phys. Rev. A* **2014**, *90*, 052521.
[23]Plasser, F.; Bäppler, S. A.; Wormit, M.; Dreuw, A. New tools for the systematic analysis and visualization of electronic excitations. II. Applications *J. Chem. Phys.* **2014**, *141*, 024107–12.
[24]Mewes, S. A.; Plasser, F.; Krylov, A.; Dreuw, A. Benchmarking excited-state calculations using exciton properties *J. Chem. Theory Comput.* **2018**, *14*, 710–725.
[25]Plasser, F.; Krylov, A. I.; Dreuw, A. libwfa: Wavefunction analysis tools for excited and open-shell electronic states *WIREs: Comput. Mol. Sci.* **2022**, *12*, e1595.
[26]Nanda, K.D.; Gulania, S.; ; Krylov, A. I. Theory, implementation, and disappointing results for two-photon absorption cross sections within the doubly electron-attached equation-of-motion coupled-cluster framework *J. Chem. Phys.* **2023**, *158*, 054102.
[27]de Wergifosse, M.; Elles, C. G.; Krylov, A. I. Two-photon absorption spectroscopy of stilbene and phenanthrene: Excited-state analysis and comparison with ethylene and toluene *J. Chem. Phys.* **2017**, *146*, 174102.
[28]de Wergifosse, M.; Houk, A. L.; Krylov, A. I.; Elles, C. G. Two-photon absorption spectroscopy of trans-stilbene, cis-stilbene, and phenanthrene: Theory and experiment *J. Chem. Phys.* **2017**, *146*, 144305.
[29]Bhattacharyya, D.; Zhang, Y.; Elles, C. G.; Bradforth, S. E. Electronic structure of liquid alkanes: A representative case of liquid hexanes and cyclohexane studied using polarization-dependent two-photon absorption spectroscopy *J. Phys. Chem. A* **2021**, *125*, 7988–7999.
[30]Bhattacharyya, D.; Zhang, Y.; Elles, C. G.; Bradforth, S. E. Electronic structure of liquid methanol and ethanol from polarization-dependent two-photon absorption spectroscopy *J. Phys. Chem. A* **2019**, *123*, 5789–5804.
[31]Sneskov, K.; Olsen, J. M. H.; Schwabe, T.; Hättig, C.; Christiansen, O.; Kongsted, J. Computational screening of one- and two-photon spectrally tuned channelrhodopsin mutants *Phys. Chem. Chem. Phys.* **2013**, *15*, 7567–7576.
[32]Hršak, D.; Holmegaard, L; Poulsen, A. S.; List, N. H.; Kongsted, J.; Denofrio, M. P.; Erra-Balsells, R.; Cabrerizo, F. M.; Christiansen, O.; Ogilby, P. R. Experimental and computational study of solvent effects on one- and two-photon absorption spectra of chlorinated harmines *Phys. Chem. Chem. Phys.* **2015**, *17*, 12090–12099.

[33]Epifanovsky, E.; Gilbert, A. T. B.; Feng, X.; Lee, J.; Mao, Y.; Mardirossian, N.; Pokhilko, P.; White, A. F.; Coons, M. P.; Dempwolff, A. L.; Gan, Z.; Hait, D.; Horn, P. R.; Jacobson, L. D.; Kaliman, I.; Kussmann, J.; Lange, A. W.; Lao, K. U.; Levine, D. S.; Liu, J.; McKenzie, S. C.; Morrison, A. F.; Nanda, K. D.; Plasser, F.; Rehn, D. R.; Vidal, M. L.; You, Z.-Q.; Zhu, Y.; Alam, B.; Albrecht, B. J.; Aldossary, A.; Alguire, E.; Andersen, J. H.; Athavale, V.; Barton, D.; Begam, K.; Behn, A.; Bellonzi, N.; Bernard, Y. A.; Berquist, E. J.; Burton, H. G. A.; Carreras, A.; Carter-Fenk, K.; Chakraborty, R.; Chien, A. D.; Closser, K. D.; Cofer-Shabica, V.; Dasgupta, S.; de Wergifosse, M.; Deng, J.; Diedenhofen, M.; Do, H.; Ehlert, S.; Fang, P.-T.; Fatehi, S.; Feng, Q.; Friedhoff, T.; Gayvert, J.; Ge, Q.; Gidofalvi, G.; Goldey, M.; Gomes, J.; González-Espinoza, C. E.; Gulania, S.; Gunina, A. O.; Hanson-Heine, M. W. D.; Harbach, P. H. P.; Hauser, A.; Herbst, M. F.; Hernández Vera, M.; Hodecker, M.; Holden, Z. C.; Houck, S.; Huang, X.; Hui, K.; Huynh, B. C.; Ivanov, M.; Jász, Á.; Ji, H.; Jiang, H.; Kaduk, B.; Kähler, S.; Khistyaev, K.; Kim, J.; Kis, G.; Klunzinger, P.; Koczor-Benda, Z.; Koh, J. H.; Kosenkov, D.; Koulias, L.; Kowalczyk, T.; Krauter, C. M.; Kue, K.; Kunitsa, A.; Kus, T.; Ladjánszki, I.; Landau, A.; Lawler, K. V.; Lefrancois, D.; Lehtola, S.; Li, R. R.; Li, Y.-P.; Liang, J.; Liebenthal, M.; Lin, H.-H.; Lin, Y.-S.; Liu, F.; Liu, K.-Y.; Loipersberger, M.; Luenser, A.; Manjanath, A.; Manohar, P.; Mansoor, E.; Manzer, S. F.; Mao, S.-P.; Marenich, A. V.; Markovich, T.; Mason, S.; Maurer, S. A.; McLaughlin, P. F.; Menger, M. F. S. J.; Mewes, J.-M.; Mewes, S. A.; Morgante, P.; Mullinax, J. W.; Oosterbaan, K. J.; Paran, G.; Paul, A. C.; Paul, S. K.; Pavošević, F.; Pei, Z.; Prager, S.; Proynov, E. I.; Rák, Á.; Ramos-Cordoba, E.; Rana, B.; Rask, A. E.; Rettig, A.; Richard, R. M.; Rob, F.; Rossomme, E.; Scheele, T.; Scheurer, M.; Schneider, M.; Sergueev, N.; Sharada, S. M.; Skomorowski, W.; Small, D. W.; Stein, C. J.; Su, Y.-C.; Sundstrom, E. J.; Tao, Z.; Thirman, J.; Tornai, G. J.; Tsuchimochi, T.; Tubman, N. M.; Veccham, S. P.; Vydrov, O.; Wenzel, J.; Witte, J.; Yamada, A.; Yao, K.; Yeganeh, S.; Yost, S. R.; Zech, A.; Zhang, I. Y.; Zhang, X.; Zhang, Y.; Zuev, D.; Aspuru-Guzik, A.; Bell, A. T.; Besley, N. A.; Bravaya, K. B.; Brooks, B. R.; Casanova, D.; Chai, J.-D.; Coriani, S.; Cramer, C. J.; Cserey, G.; DePrince, A. E.; DiStasio, R. A.; Dreuw, A.; Dunietz, B. D.; Furlani, T. R.; Goddard, W. A.; Hammes-Schiffer, S.; Head-Gordon, T.; Hehre, W. J.; Hsu, C.-P.; Jagau, T.-C.; Jung, Y.; Klamt, A.; Kong, J.; Lambrecht, D. S.; Liang, W.; Mayhall, N. J.; McCurdy, C. W.; Neaton, J. B.; Ochsenfeld, C.; Parkhill, J. A.; Peverati, R.; Rassolov, V. A.; Shao, Y.; Slipchenko, L. V.; Stauch, T.; Steele, R. P.; Subotnik, J. E.; Thom, A. J. W.; Tkatchenko, A.; Truhlar, D. G.; Van Voorhis, T.; Wesolowski, T. A.; Whaley, K. B.; Woodcock, H. L.; Zimmerman, P. M.; Faraji, S.; Gill, P. M. W.; Head-Gordon, M.; Herbert, J. M.; Krylov, A. I. Software for the frontiers of quantum chemistry: An overview of developments in the Q-Chem 5 package *J. Chem. Phys.* **2021**, *155*, 084801.

[34]Krylov, A. I.; Gill, P. M. W. Q-Chem: An engine for innovation *WIREs: Comput. Mol. Sci.* **2013**, *3*, 317–326.

[35]Kamarchik, E.; Krylov, A. I. Non-Condon effects in one- and two-photon absorption spectra of the green fluorescent protein *J. Phys. Chem. Lett.* **2011**, *2*, 488–492.

[36]Krylov, A. I. From orbitals to observables and back *J. Chem. Phys.* **2020**, *153*, 080901.